Monitoring the Cold Spray Process

Real-Time Particle Velocity Monitoring Through Airborne Acoustic Emission Analysis

Koufis, Stratos; Eskue, Nathan; Zarouchas, Dimitrios; Pascoe, John Alan

DOI
10.1007/s11666-024-01878-1

Publication date
2024

Document Version
Final published version

Published in
Journal of Thermal Spray Technology

J Therm Spray Tech
https://doi.org/10.1007/s11666-024-01878-1

ORIGINAL RESEARCH ARTICLE

Monitoring the Cold Spray Process: Real-Time Particle Velocity Monitoring Through Airborne Acoustic Emission Analysis

Stratos Koufis[1] · **Nathan Eskue**[1] · **Dimitrios Zarouchas**[1] · **John-Alan Pascoe**[1]

Submitted: 3 July 2024 / in revised form: 29 October 2024 / Accepted: 29 October 2024

Abstract Continuous monitoring of spray velocity during the cold spray process would be desirable to support quality control, as spray velocity is the key process parameter determining the deposit quality. This study explores the feasibility of utilising Airborne Acoustic Emission (AAE) for real-time monitoring of spray velocity. Six spray tests were conducted, varying pressure and temperature to achieve different velocities. Optical means were used to measure velocity; while, the signal from the AAE was captured during deposition via a microphone. Features demonstrating a strong correlation with velocity were extracted from the acoustic signals. Both rule-based and machine learning models were employed to identify the moments where the nozzle was engaged with the substrate and diagnose the velocity. The results indicate that monitoring the spray velocity of the cold spray process using AAE is feasible.

Keywords acoustic emission · cold spray · machine learning · particle velocimetry · process monitoring

Introduction

The cold spray process, an emerging additive manufacturing technique, accelerates metallic powder particles at supersonic velocities through a converging–diverging nozzle using a carrier gas. Upon impact with a substrate, it forms a dense, adherent deposition favourable for coating and repair applications. Its advantages include low-temperature operation, minimal oxidation, and reduced thermal degradation, making it particularly appealing for the aerospace, automotive, and maritime industries (Ref 1-5).

Reliable process monitoring of cold spray is crucial for ensuring robust quality control and advancing the development of a fully automated process. Among the many process parameters that can be controlled directly or indirectly, it has been found that the impact velocity and particle temperature govern the quality of the deposit. (Ref 6, 7). Regarding the effort of monitoring the process, ultrasonic acoustic techniques have been used to diagnose coating thickness buildup (Ref 8). Thermocouples and infrared cameras have been employed successfully to acquire data in line with the process (Ref 6, 9-11). Particle velocimetry techniques have also been used to diagnose the particle velocity at the exit of the nozzle (Ref 12, 13). In addition, other optical methods have been proposed to extract the characteristics of the micro-particle motion (Ref 14, 15). The most crucial drawback of the particle velocimetry techniques is the difficulty of implementation during the actual spraying of the component due to the relatively short spray distance of the process and the bulky monitoring equipment available today.

Airborne acoustic emission (AAE) is a promising alternative technique for monitoring the cold spray particle velocity and the cold spray process in general due to its non-intrusive nature. AAE has been used to monitor industrial equipment and diagnose process anomalies successfully, and when combined with statistical and machine learning models, it is a powerful tool for process monitoring (Ref 16). Regarding AAE monitoring of the thermal spray process, Burkert et al. (Ref 17) used AAE to identify when clogging appeared inside the nozzle. Duan et al. correlated the health condition of the anode with the power

✉ Stratos Koufis
e.koufis@tudelft.nl

[1] Faculty of Aerospace Engineering, Delft University of Technology, Delft, The Netherlands

Published online: 14 November 2024

spectrum of the acoustic signal captured during the process of plasma spray (Ref 18). Kamnis et al. (Ref 19) diagnosed the microhardness of a thermal sprayed coating with the help of a multilayer perceptron (MLP) for a varying powder feed rate and standoff distance using AAE. Malamousi et al. (Ref 20) classified sound samples of different thermal spray experiments according to the powder feed rate. These examples illustrate that AEE can provide detailed information about various aspects of the thermal spray process, including equipment health, process parameters, and material properties of the deposit. It is hypothesised that AAE could similarly be applied to the cold spray process to address similar challenges due to the similarities between the two processes. However, no work is available where AAE has been applied to cold spray.

Developing an acoustic system for process monitoring starts with data acquisition. This involves capturing signals from acoustic sensors placed strategically within the system. Then, the raw signals (time domain) can be directly utilised or subjected to signal decomposition techniques to analyse their frequency content. The feature extraction step follows and involves deriving statistical metrics from the signals in different domains (time, frequency, time-frequency). Another approach is directly using the raw signal as input for the machine learning models. Additionally, a combination of both statistical metrics and raw signals can be used simultaneously (Ref 16).

These features or raw signals are used as input for machine learning models, often neural networks, widely used for classification or regression tasks. Neural networks consist of interconnected nodes usually organised in layers. Each node performs simple computations, and the connections between nodes allow information to flow through the network. During training, a neural network learns to adjust its parameters based on the input data, aiming to make accurate predictions (Ref 21).

Neural networks have been used with acoustic data in different applications, including diagnostics and prognostics. Diagnostics help identify process conditions and the health state of a system that can either be healthy or faulty (Ref 16) or even quantify the health state using a health indicator. Meanwhile, in prognostics, they predict outcomes like the remaining useful life of a system (Ref 22-24). For the case of cold spray, such an acoustic system would have the potential to perform a real-time diagnosis of the spray velocity, identify process anomalies, and diagnose the health state of critical components such as the spray nozzle.

This work aims to investigate the feasibility of AAE in monitoring the particle velocity in the cold spray process. A feature exploration from the acoustic signal is performed to identify features significantly correlating with the particle velocity. A methodology was also developed to determine the process segments where the nozzle is engaged with the substrate, and for those moments, velocity diagnosis was performed.

Experimental Procedure

Cold Spray Process and Particle Velocity Measurements

The selected material system was an aluminium alloy 6061 substrate and the AM103 aluminium powder from VALIMET (Stockton, California, USA), which, according to the manufacturer's specifications (Ref 25), has the chemical composition reported in Table 1. As per the same specifications, the particle size distribution indicates that 90% of the particles had a diameter below 52 µm, 50% below 34 µm, and 10% below 1 µm. The substrate material was made of flat plates with a thickness of 3 mm that were sandblasted before the deposition to improve adhesion. The aim was to create a deposition with dimensions of approximately 45x30 mm, with the thickness being an output of the experiment.

A high-pressure cold spray system (PCS-1000) from Titomic Europe (Akkrum, The Netherlands) was employed for the tests. A PBI (Polybenzimidazole) nozzle was used. To achieve uniform deposition, the path of the nozzle extends beyond the edges of the specimen so that the starting and ending points of each pass do not lie within the surface of the specimen; this is called overspray. Three layers were deposited, each consisting of 20 parallel passes, resulting in 60 passes in total. The spray path is shown in Fig. 1. The standoff distance was 25 mm, and the powder feeder was set to 3 rpm.

A sensitivity analysis was performed concerning temperature and pressure to create deposits with different spray velocities. The goal was to achieve velocities above the

Table 1 Chemical composition of the powder used for tests

Al	Si	Mg	Fe	Mn	Ti	Zn	Cu	Others (each)	Others (total)
Balance	9.0-11.0%	0.25-0.45%	< 0.40%	0.15%	< 0.15%	< 0.10%	< 0.03%	< 0.05%	< 0.15%

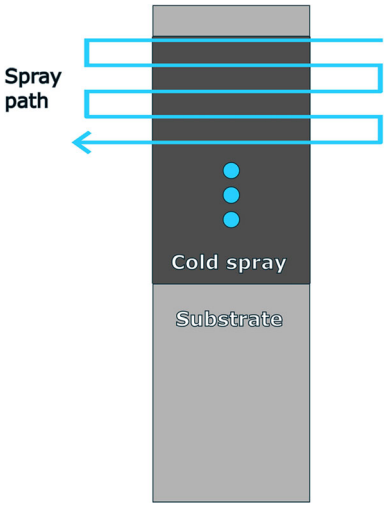

Fig. 1 Spray path that was followed during the experiments. To achieve a uniform deposition, the start and end points were not within the specimen (overspray)

critical for deposition velocity, about 600 m/s (Ref 26, 27) to produce acoustic data simultaneously and investigate the possibility of velocity diagnosis. Six experiments were performed. For four experiments, the temperature was kept constant at 600 °C, and the selected pressures were 3.5, 4.5, 6, and 7 MPa. Two additional experiments were conducted with the pressure set to 5 MPa for both; while, the temperatures were set to 400 and 500 °C, respectively. This sensitivity analysis also aimed to investigate if features that are not sensitive to pressure and temperature separately but are affected only by the resulting spray velocity can be extracted from the AAE, irrespective of how this velocity was achieved.

A commercial system containing a laser to Illuminate particles and a high-speed camera was used to measure particle velocity via the particle image velocimetry method. Before each test, the nozzle was positioned in front of the camera, and the average particle velocity was measured at a distance from the nozzle tip equal to the standoff distance (25 mm). Then, the nozzle was moved to the spray position, and cold spray was performed. The deposition lasted approximately 70 s. Therefore, the assumption was made that the average particle velocity remained constant throughout the deposition.

AAE Data Acquisition

An M51 microphone (1/2-inch condenser pre-amplified) from LinearX Systems (Tualatin, Oregon, USA) was used to capture the airborne acoustic emission of the process. The microphone was placed at 1870 mm from the centre of the substrate to minimise any effect of the small displacement of the nozzle relative to the distance from the microphone. The microphone exhibits an almost flat response for frequencies between 20 Hz and 20 KHz, with a slight drop for higher frequencies. The maximum sound pressure level is 150 dB to ensure no distortion while recording such a loud process. The microphone shows high directionality for sound waves with an incidence angle higher than $\pm$ 15°, so it was placed at 90° from the spray plume, aiming to capture mainly the sound coming from the nozzle-substrate system, reducing the ambient noise. A calibration pistonphone was used to calibrate the microphone with a sound wave of frequency 250 Hz and amplitude 114 dB. The microphone's response was found to be 0.0152 V/Pa of sound pressure. A DC power supply was used with the microphone, and the output voltage was set at 9.15 V. The PicoScope 5443D data acquisition system from Pico technology (Cambridgeshire, UK) was used to convert the analogue signal to digital with a sampling rate of 50 KHz. A schematic of the experimental setup is shown in Fig. 2

Results and Discussion

Sprayed Specimens, Measured Spray Velocity and AAE Acquisition

Successful deposition was achieved in all six tests/specimens, as was expected based on the deposition window of this material (Ref 26, 27). Figure 3 shows the top view of the sprayed specimens. The measured spray velocities were from 580 to 690 m/s and are summarised in Table 2. While performing particle velocimetry for test 6, the velocity was less stable than for the rest of the experiments, and the value of 600 m/s was taken as an average value of that fluctuation.

An important effect to consider regarding the velocity measurements is the bow shock phenomenon. The bow shock phenomenon occurs when the supersonic flow encounters an obstacle, creating a shock wave that reduces the particle velocity. This can lead to a reduction in particle velocity just before impact, directly influencing deposition quality. The analysis in this study did not consider the effect of the bow shock because the particle velocimetry was performed without a substrate. While the bow shock effect may indeed be present at the selected spray distance, leading to a potential overestimation of the actual impact velocity, we assume that its influence is constant across measurements. However, for more precise velocity determination, an additional correction is be necessary to account for the bow shock's influence on the measured velocities. Computational fluid dynamics (CFD) simulations could be used to make this correction (Ref 28).

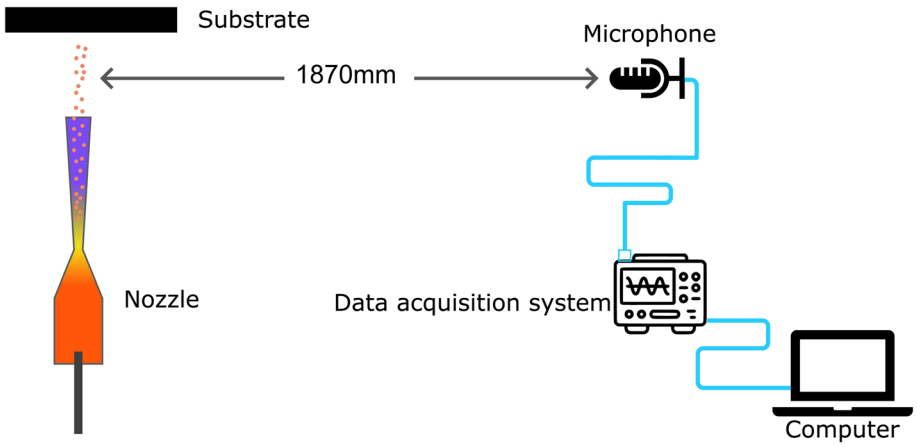

Fig. 2 Experimental setup used to capture the signal from the AAE of the cold spray process

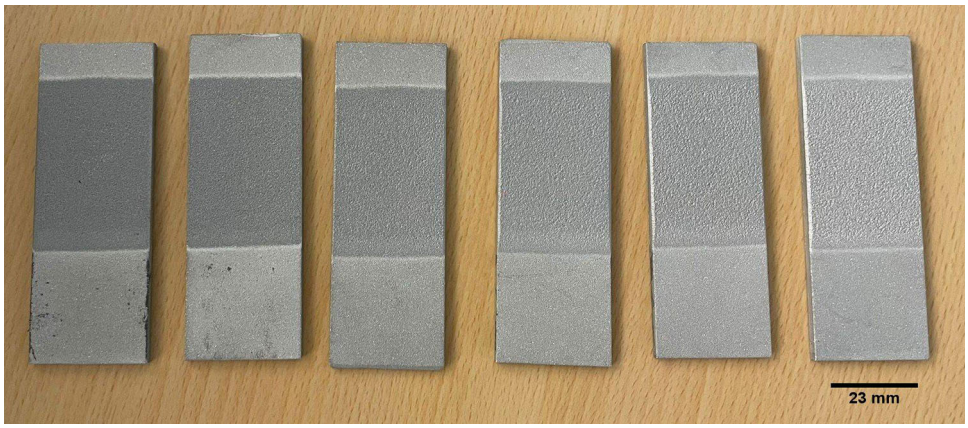

Fig. 3 Top view of the cold-sprayed specimens from the six tests

Table 2 Pressure temperature and average particle velocity of the experiments performed

Test	Pressure, MPa	Temperature, °C	Average particle velocity, m/s
1	6	600	670
2	4.5	600	625
3	7	600	690
4	5	500	620
5	3.5	600	580
6	5	400	600

A short representative segment of the AAE's raw signal captured by the microphone is shown in Fig. 4. The vertical axis indicates the pressure of the acoustic wave (fluctuation from the ambient pressure). The parts of spray and over-spray are also visible in the same figure, each with a duration of approximately 0.55 s. Due to a malfunction of the data acquisition system, only the first 24 s were captured for the first experiment.

Feature Extraction from the Whole Raw Signal

The first step of the investigation was to extract features from the raw signal. A sliding time window of 3 s was used with a stride of 1 s. This time window was chosen to ensure that the extracted features exhibited minimal variation over time, indicating that the time window contained representative data of the process conditions. Among the different features examined in the time domain, root mean square (RMS) (Eq 1) exhibited a clear trend with velocity, with x_i being the value of the discrete signal at the moment i and N is the length of the time window.

$$\mathrm{RMS} = \sqrt{\frac{1}{N}\sum_{i} x_i^2} \qquad \text{(Eq 1)}$$

The RMS of the signal throughout the six tests is shown in Fig. 5. The average per test RMS is demonstrated in Fig. 6. Both figures show that RMS tends to increase with

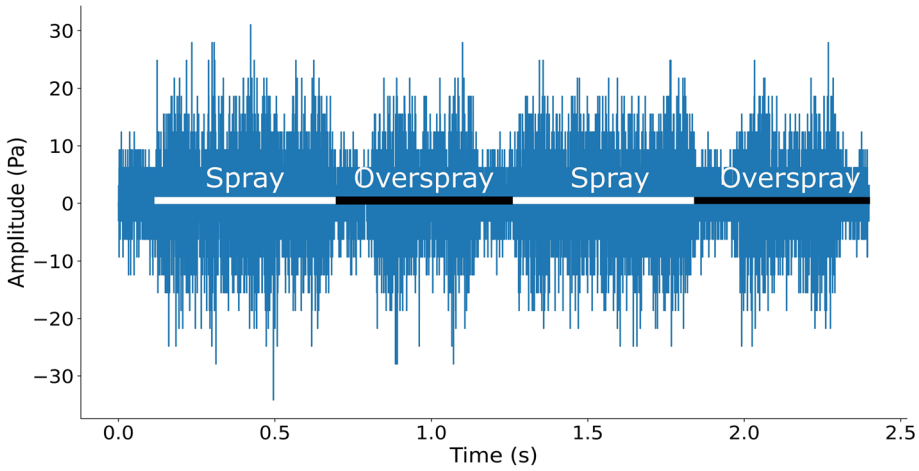

Fig. 4 Segment of the raw signal from the cold spray process. The amplitude indicates the measured pressure fluctuation from the ambient pressure caused by the acoustic wave. The spray and overspray parts of the segment are highlighted

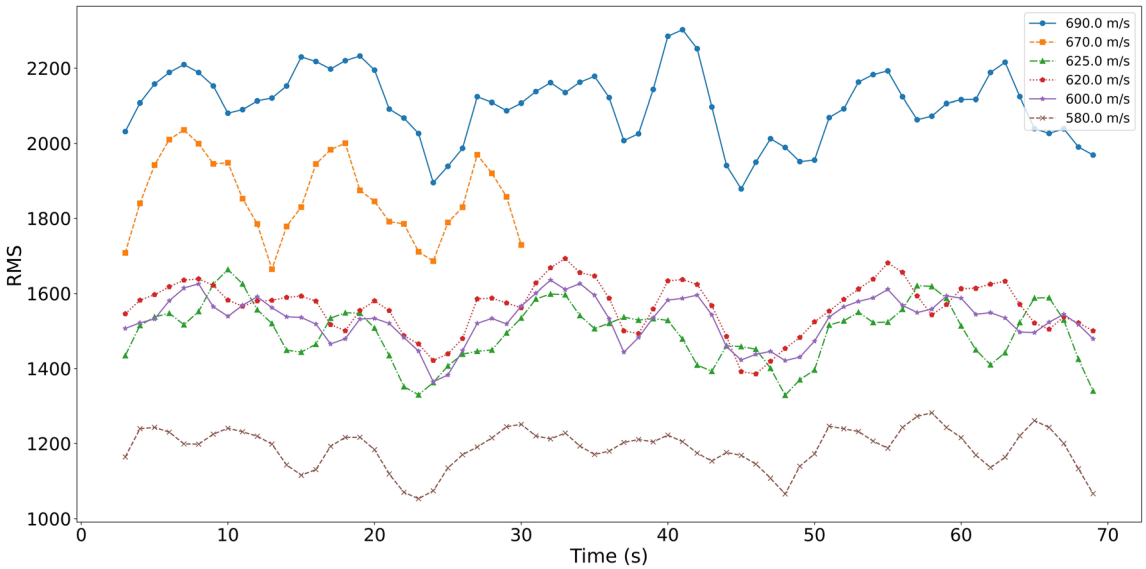

Figure 5 RMS of the raw signal for the different tests for a time window of 3 s with a stride of 1 s

increasing spray velocity. Both the spray and overspray segments were used for the feature extraction, and the RMS showed that it is informative of the spray velocity. A simple statistical model has the potential to be used to monitor particle velocity in standardised cold spray applications, such as in an industrial line where a specific number of cold spray deposits with known dimensions and material systems are performed. Such a model would be able at least to identify permanent shifts in the spray velocity reflected on the signal's RMS. However, it has two significant limitations: (1) the large time window that cannot catch short-duration events that can be detrimental to the quality of the deposit and (2) that it is specific to a single type of substrate and not flexible to spray on substrates with different geometries due to the different sequence of spray/overspray segments that it would introduce. To develop a generalised model, it is essential to identify the segments where the spray is performed and examine them separately.

Time Windowing

In this study, every spray and overspray event lasted approximately 0.55 s. A time window of 0.11 s was selected allowing the model to capture more diagnostic steps for a given sound segment of a specific duration. This short time window ensures that the model can effectively capture the frequent transitions between spray and overspray conditions. However, a time window of 0.11 s was too small to capture comprehensive information for accurate diagnostics. An overlap of 0.22 s with the previous and the next time windows was introduced to address this challenge (Fig. 7). This overlap extends the analysis span to 0.55 s, providing a larger window for monitoring the

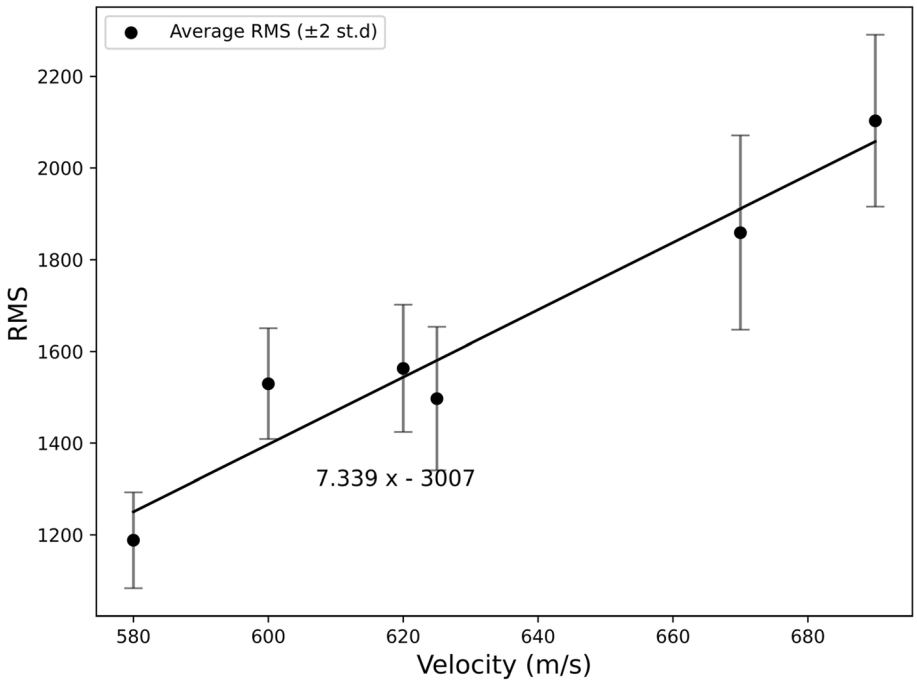

Fig. 6 Average RMS per experiment shows a positive correlation with velocity

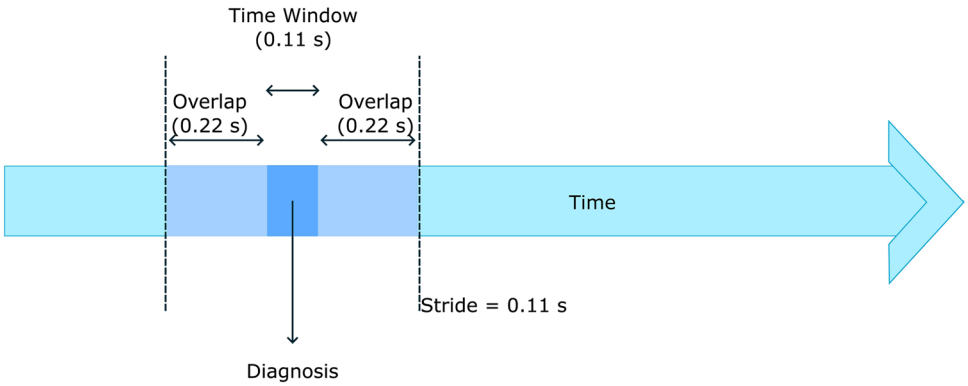

Fig. 7 Time window used to perform diagnostics

process while retaining the high resolution of the 0.11-second windows.

Feature Extraction Separating Spray from Overspray Segments

All the spray and overspray segments of the signal acquired from the AAE were separated manually, and statistical features were extracted from both the time and frequency domain. The aim was first to extract features that distinguish spray from overspray. Then, features that show a clear trend with spray velocity were identified for the spray segments.

The RMS (Eq 1) and the zero crossing rate (Eq 2) were selected where x represents the signal sample at time instant i. In Fig. 8, it is shown that the average RMS of the spray segments of each experiment shows a positive correlation with the spray velocity. The largest error from the linear interpolation is for the last experiment of 600 m/s, which showed instability in its velocity. Furthermore, the average zero crossing rate can separate spray from overspray segments in the examined velocity domain by setting a threshold.

$$\begin{aligned} \mathrm{ZCR} &= \frac{1}{2N}\sum_{i=1}^{N-1}|\mathrm{sgn}(x_{i+1}) - \mathrm{sgn}(x_i)| \text{with } \mathrm{sgn}(x) \\ &= \begin{cases} 1 & if\ x > 0 \\ 0 & if\ x = 0 \\ -1 & if\ x < 0 \end{cases} \end{aligned} \quad \text{(Eq 2)}$$

A Fast Fourier Transform (FFT) was performed at each spray segment of a length of 0.55 s to extract features from the frequency domain. Then, the power spectral density

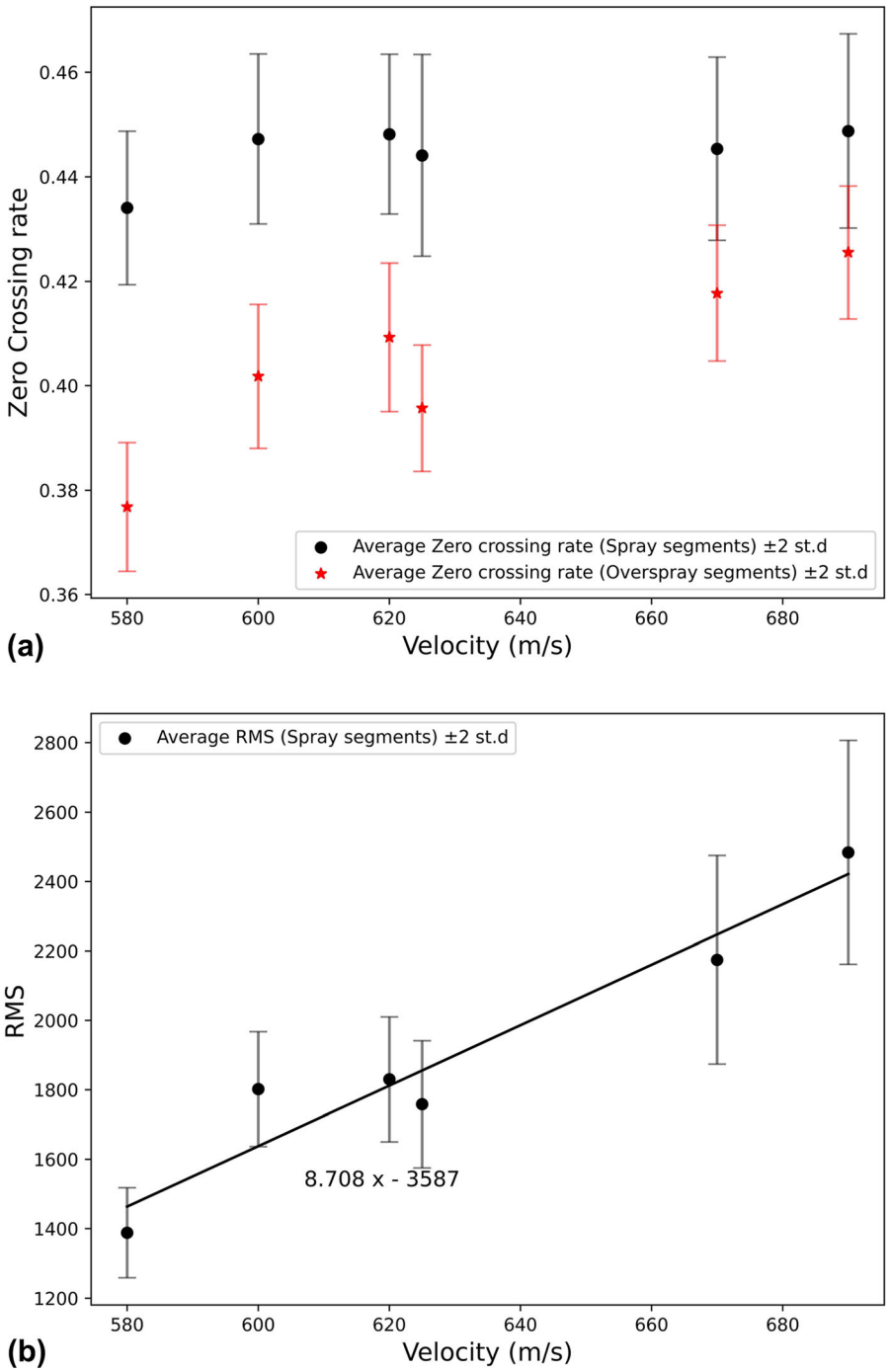

Fig. 8 (a) Zero crossing rate (with two standard deviations) of the spray and overspray segments can be used to separate these two conditions. (b) The average RMS of the spray segments (with two standard deviations) shows a positive correlation with the spray velocity

(PSD) was calculated to investigate how the power of the signal is distributed among the frequencies. This analysis aimed to identify dominant frequency peaks and observe potential changes in their amplitudes or shifts within the frequency domain as the spray velocity increases. The PSD was calculated through (Eq 3) where P_f is the magnitude of the complex number that the FFT outputs and corresponds to a single frequency bin, F_r is the sampling rate, and Δ is the number of points in the time window. By dividing F_r by Δ, the frequency resolution of the FFT is calculated along with the length of the frequency bin. So, the power is normalised per Hz of the frequency bin.

$$\mathrm{PSD} = \frac{P_f^2}{F_r/\Delta} \qquad \text{(Eq 3)}$$

Fig. 9 plots the average PSD of all the spray segments per test. The power increases with increasing velocity, as shown from the RMS of the time domain signal. The power

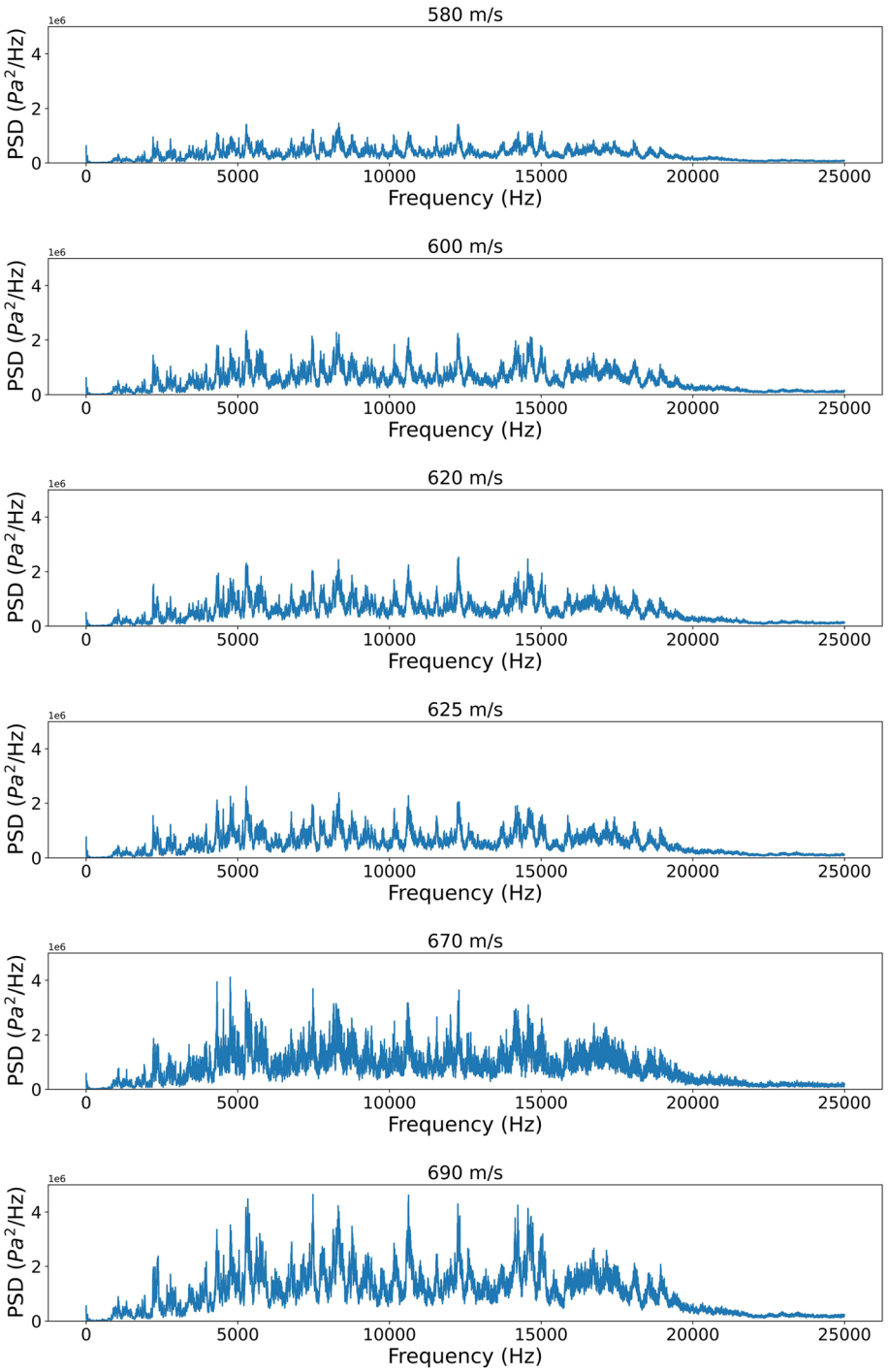

Fig. 9 Averaged PSDs of all the tests performed. Frequency shifts are not apparent; power increases gradually with velocity

peaks do not show any apparent frequency shift for different velocities.

Since the PSD increased gradually with increasing velocity, a Pearson correlation analysis was performed to identify frequency bands demonstrating a high linear correlation with the velocity. To do that, the resolution of the PSD was reduced to approximately 26 Hz. The averaged PSDs of every test were correlated with the velocity. It was found that 17 frequency bins scored higher than 0.99, meaning a highly linear relationship, as shown in Fig. 10. Although the average PSD of each experiment scored high in Pearson correlation, implying that a simple linear relationship could calculate the velocity from the power of specific frequency bins, the standard deviation of the samples from every experiment is so high that it makes it difficult to use a straightforward model for velocity diagnosis, as is depicted in Fig 11.

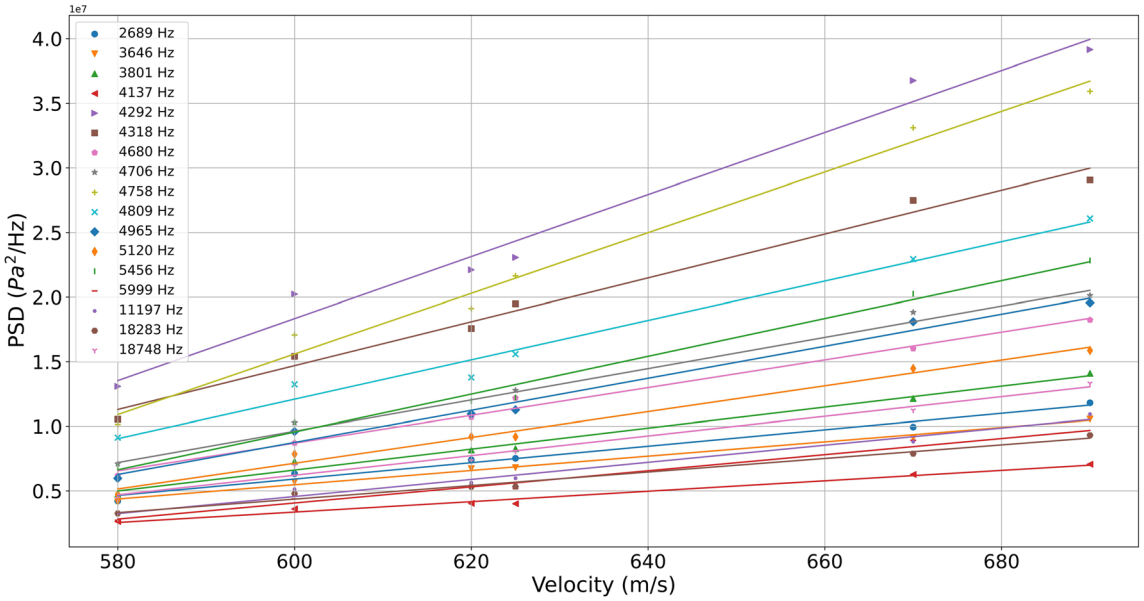

Fig. 10 Frequencies that scored high in Pearson correlation analysis and exhibit an almost linear relationship with velocity

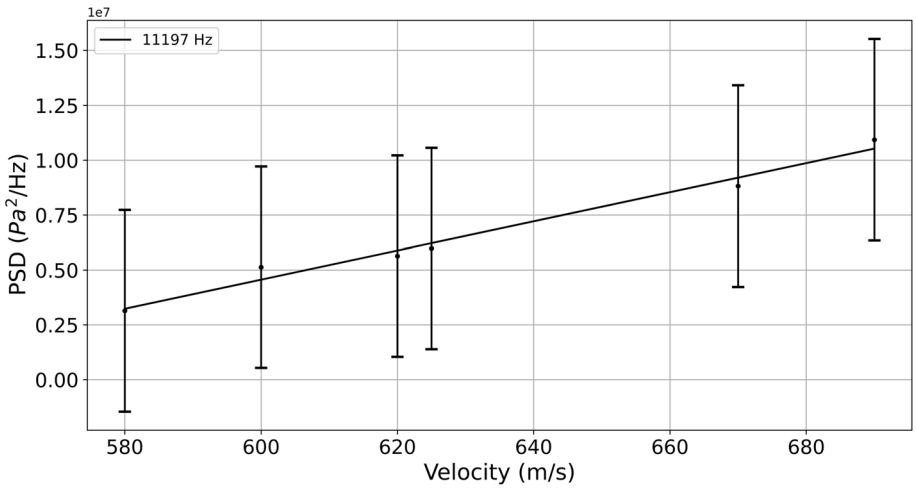

Fig. 11 Example of the power of the frequency of 11197 Hz with respect to the spray velocity. The average values exhibit a linear relationship. Two standard deviations are also shown

The PSDs of experiments 4 (620 m/s) and 6 (625 m/s) were plotted on top of each other for comparison (Fig. 12). For these two experiments, almost the same spray velocity was achieved with a different combination of pressure and temperature. The average PSDs match well enough, implying that features that are agnostic of the pressure and temperature separately and only depend on the velocity can be extracted.

Process Diagnostics

To perform process diagnostics, it is essential to identify the spray segments. A threshold of 0.43 on the zero crossing rate (ZCR) was used to achieve that. This was the middle point between the minimum ZCR of the spray segments and the maximum ZCR of the overspray segments (Fig. 8). A zero crossing rate higher than 0.43 indicates the spray condition. The time window described in the previous section (Fig. 7) was used to investigate the signal acquired from all six experiments. This statistical algorithm correctly classified 83% of the experiments' time windows. Although this model is simple and performed well, it is very specific to the domain examined and highly dependent on the data from the overspray condition. This highlights the need for a model that identifies the spray condition while being agnostic of the overspray condition.

Considering the determination of the velocity through the RMS or the PSD, both failed to give an accurate model that either performs regression or classification to low (580-600 m/s) medium (620-625 m/s) high (670-690 m/s) spray velocity. The high standard deviation of those features during the same experiment posed a challenge,

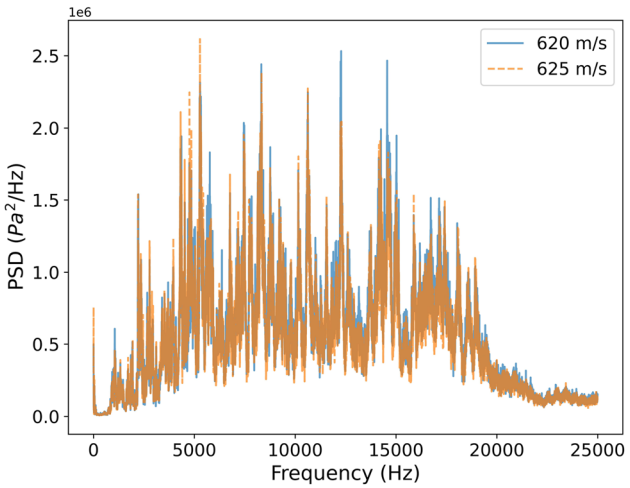

Fig. 12 Comparison of PSD between experiments of 620 and 625 m/s using different combinations of pressure and temperature; no significant differences are apparent, implying that features that are only dependent on the velocity can be extracted

resulting in substantial overlap among the features across different operating conditions. Consequently, a linear rule-based model could not diagnose velocity based on those features.

The feature extraction successfully classified spray and overspray segments. However, a more generic model that identifies spray segments and distinguishes them from anything else would be desirable. Therefore, an autoencoder was employed to determine the spray segments. An autoencoder is an artificial neural network used for unsupervised learning tasks. It consists of two main components: an encoder and a decoder. The encoder compresses the input data into a lower-dimensional representation, capturing the most important features of the input. This compressed representation retains the essential information and discards irrelevant details. The decoder then takes this compact representation and reconstructs the original input data as precisely as possible. During training, the autoencoder learns to minimise the reconstruction error by tuning its parameters to produce accurate reconstructions (Ref 16).

An autoencoder was trained only with the spray segments from different velocities. As a result, a high reconstruction error was expected when the autoencoder receives as input a segment where overspray takes place (or any condition other than normal spray condition). Then, the reconstruction error can be used to classify the process condition (spray or not).

To reduce the data size and thus the complexity required from the autoencoder to perform an accurate reconstruction, the same frequency bins of 26 Hz applied in Pearson correlation analysis were used. Due to the large magnitude of the PSD values, they were normalised using their mean value per spray sample. This was done to ensure the stability of the training process.

The autoencoder consists of a convolutional layer with ten filters, each with a kernel size of 5 and a stride of 1. A flattening layer is added to concatenate the output of the convolutional layer to a one-dimensional array that can then be used as input to a fully connected layer of 20 neurons. The bottleneck layer consists of 10 neurons. The rest of the network is symmetric to the bottleneck layer. The hyperparameters of the network were selected empirically, and no optimisation algorithm was used. A mean square error (MSE) loss function is used to calculate the reconstruction error between input and output (Eq 4). To calculate MSE, n is the number of frequency bins of the PSD of a sample, y_i is the value of the PSD of the *ith* frequency bin and $\widehat{y_i}$ is the reconstructed value of the PSD of the same frequency bin. Leaky Rectified Linear Unit (LReLU) was used as an activation function with a negative slope of 0.2 (Ref 29), and the Adam optimiser (Ref 30) was used to update the learnable parameters after each epoch. A batch size of 40 was used for training. The network architecture and the hyperparameters are summarised In Fig. 13.

$$\text{MSE} = \frac{1}{n}\sum_{i=1}^{n}(y_i - \widehat{y_i})^2 \qquad \text{(Eq 4)}$$

To test the performance of the autoencoder, 10% of the spray dataset was kept as test data. This is data that the network does not see during training and is used for evaluation. From the remaining spray data, 80% was used as train data, which is the data used to update the learnable parameters of the network and 20% as validation, which is data that the network does not see during training and is used to monitor its performance on unseen data during training.

The training was stopped when the validation loss was not decreased for 15 consecutive epochs, and the last model that showed a decrease was kept. The average reconstruction MSE on the test data was 0.181, with a standard deviation of 0.025. The reconstruction loss of the overspray segments—which the network was not trained on—was also plotted along with the training and validation loss in Fig. 14. This gave a better overview of the ability of the network to separate spray from overspray based on the reconstruction error.

To further validate the robustness of the autoencoder, a whole experiment was kept entirely out of the training dataset and was used as test data. Then, from the remaining data, an 80-20 split was used for training and validation data, respectively. With this, it was ensured that the model does not memorise the segments of each experiment but extracts essential information that makes it able to

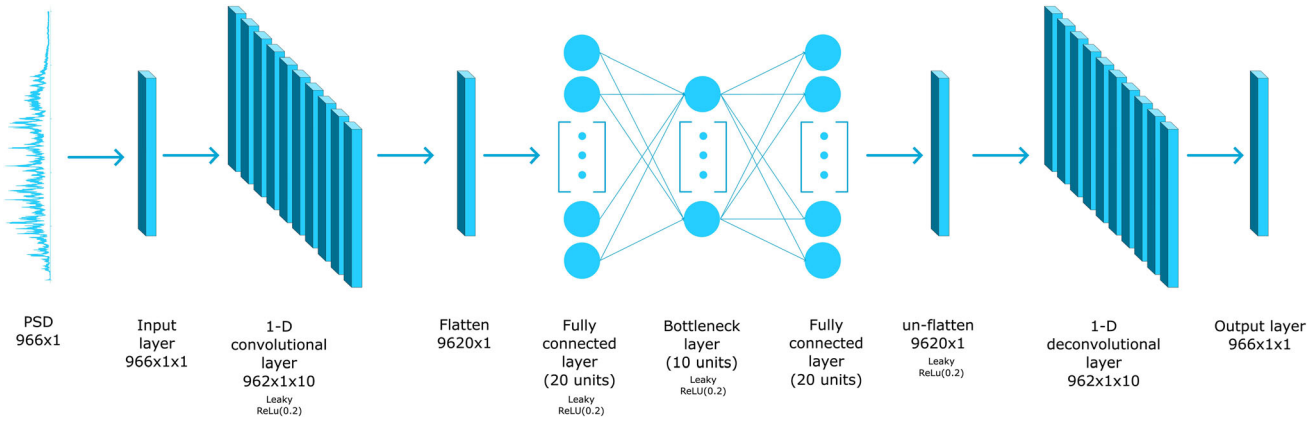

Fig. 13 Autoencoder architecture that was trained with spray segments of different velocities aiming to separate spray from overspray condition based on the reconstruction error

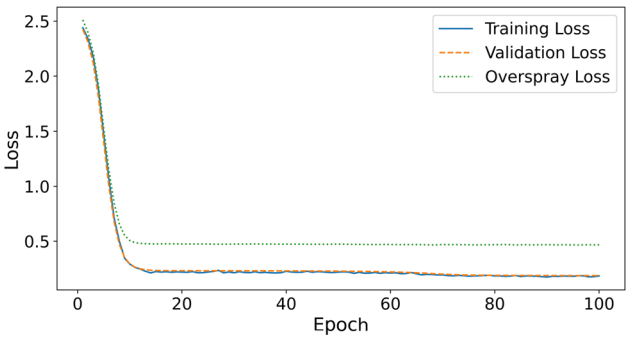

Fig. 14 Autoencoder learning curve. The reconstruction loss of the overspray segments is also shown to evaluate the ability of the autoencoder to separate spray from overspray segments based on the reconstruction error

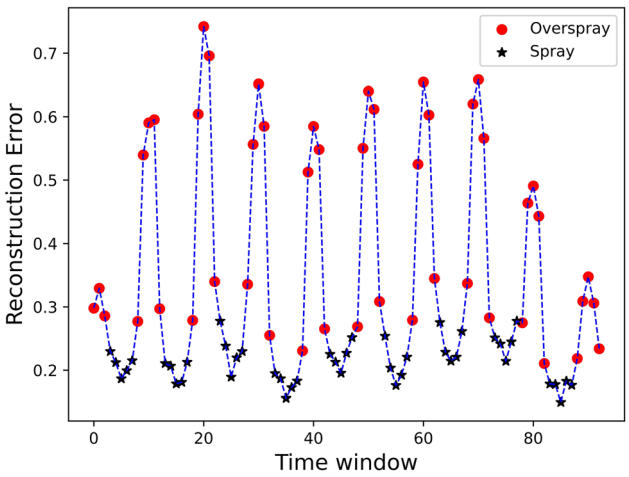

Fig. 15 Evolution of the reconstruction loss of the autoencoder when transition from spray to overspray takes place

Table 3 Validation of the autoencoder model, where Test X refers to the experiment that was used as test data to evaluate the algorithm performance

Test kept out	Test 1	Test 2	Test 3	Test 4	Test 5	Test 6
Training loss	0.167	0.179	0.181	0.172	0.184	0.193
Validation loss	0.177	0.188	0.455	0.177	0.183	0.189
Test loss	0.190	0.192	0.190	0.180	0.182	0.190
Test loss st.d.	0.032	0.031	0.035	0.017	0.020	0.033
Overspray loss	0.392	0.448	0.455	0.398	0.043	0.451

generalise for cold spray tests performed with spray velocities that the algorithm was never trained with. The results are presented in Table 3. The reconstruction error was kept low no matter which test was kept out, even if it was the two limit values of the domain (580 and 690 m/s). This means the model is generalised, at least in the examined domain (580-690 m/s).

All six signals acquired from the AAE of the six experiments were tested with the autoencoder using the sliding window explained above, and the goal was to classify each time window to spray or overspray. Five different but random weight initialisations were tested to ensure the robustness of the autoencoder. The training process was performed as previously described for each initialisation. After each model was trained, the value of the average test reconstruction error and its standard deviation were used to set a threshold that effectively distinguishes between spray and overspray. That threshold was the average reconstruction error on the test data plus two standard deviations (st.d.). For the five different initialisations, the average accuracy of time windows in which the condition was diagnosed correctly was 84%, with a standard deviation of 1%. As explained above, the case study was considered an extreme case where the transition between the two conditions happens frequently, so the accuracy is considered satisfactory.

To explain better how the classification based on the reconstruction error works, in Fig. 15, the reconstruction error for the first 100 time windows of the signal of test 4 is presented as an example. The spray and overspray time windows are also labelled in the same figure. For the experiments of this work, a time window requires five strides to scan a whole spray segment and another five to scan the following overspray segment. At the first stride, the total time window (including overlap) used as input for the autoencoder consists of 60% spray condition but also includes 40% of the overspray condition. At the next stride, the total time window contains 80% spray and 20% overspray. At the third stride, 100% spray. At the fourth stride, 80% spray and 20% overspray; at the fifth and final stride, 60% spray and 20% overspray. Among the five time windows it takes until the transition from spray to overspray, the error reaches a minimum when the time window, including the overlap, coincides with the pure spray condition and increases as noise from the transition is introduced. Despite introducing noise from the overlap, the variation of the reconstruction error for the spray segments shows a slight fluctuation. This makes it possible to separate the two conditions by setting a simple threshold at the reconstruction error. The reconstruction error can also be helpful in an automated process so that the system can be informed about the transition from spray to overspray before this happens.

The final step is to perform a velocity diagnosis on the spray segments. This was done by employing an MLP. A multilayer perceptron (MLP) is a specific type of neural network characterised by multiple layers of nodes, including an input layer, one or more hidden layers, and an output layer. Each node in a layer is connected to all nodes in the next layer. The MLP is trained by adjusting its parameters, called weights and biases, across these layers. These adjustments allow the network to capture complex patterns in the data. Like other neural networks, MLPs are often used for classification and regression tasks, learning from the input data to make predictions. The resolution of the frequency bins remained at 26 Hz since frequency bins of this size were found to score high in Pearson correlation with velocity. Furthermore, an MLP can extract higher-order relations between the PSD bins and the velocity. The first 50 and the last 200 frequency bins were removed from the PSD since the bands 0-1294 Hz and 19824-25000 Hz seemed to contain little information, and the microphone exhibited a drop in its response above 20 kHz.

The aim was to perform a three-class classification into low (580-600 m/s), medium (620-625 m/s), and high (670-690 m/s) velocity. The classification aimed at establishing a framework for using airborne acoustic emission (AAE) signals for cold spray velocity diagnostics. The absence of velocities between the classes reflects the limited experimental data available at this stage. As more data are collected, it is expected to refine the model, potentially moving towards a continuous classification or a regression approach. The architecture of the MLP is shown in Fig. 16. The neural network consists of a series of three dense

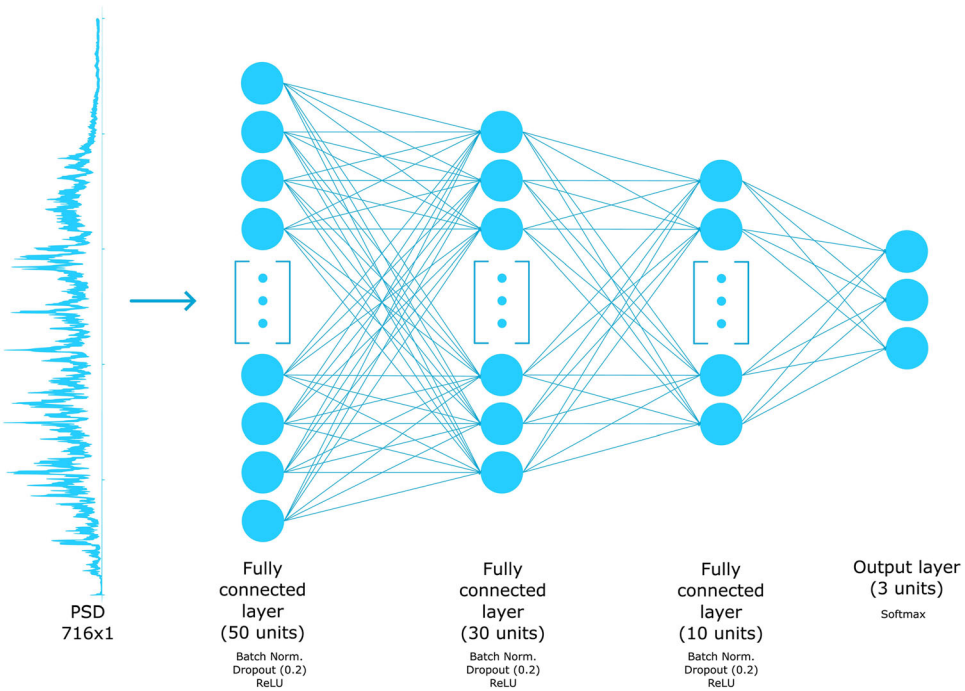

Fig. 16 MLP for classification of the spray segments according to their spray velocity

layers with batch normalisation (Ref 31) and a dropout layer (Ref 32) following every dense layer to increase the stability of the training process and avoid overfitting. The Rectified Linear Unit (ReLU) function was used as an activation function (Ref 24) for the hidden layers. A SoftMax activation function was used for the last layer to convert the neuron's output to probabilities belonging to each class (Ref 33). The Adam optimiser (Ref 25) was used to update the learnable parameters after each epoch with a learning rate of 0.005.

20% of the spray segments were kept as test data, and the remaining dataset was split into 80% train data and 20% validation data. A batch size of 40 was used for training. Again, the hyperparameters of the network were selected empirically, and no optimisation algorithm was used. The training was done five times for five different but random weight initialisations to evaluate stability. The average confusion matrix of the test set with the standard deviation is shown in Fig. 17. The confusion matrix shows the true labels of the test dataset and the labels that the machine learning algorithms assigned to those segments. The result showed that the MLP could accurately identify the high-velocity class. However, there is some confusion among the first two classes. It is believed that the spray velocity instability observed during the fifth experiment (600 m/s) affected the training process. Based on the RMS (Fig. 8) and the PSD (Fig. 9) of this experiment, it can have features that can be characteristics of both "low" and "high" classes, making the classification task challenging. Furthermore, the first and the second classes are closer in terms of velocity range than the second and the third, making it more possible to share similar features.

It should be noted that at present the velocity classification is based on the velocity measured through the optical particle velocimetry; while, the actual impact velocity may be affected by the bow shock phenomenon. Therefore, in future, to improve the accuracy of AAE-based monitoring, it is essential to incorporate corrections for the bow shock effect when relevant. In most cases, the standoff distance is known, and CFD simulations can model and quantify the velocity reduction caused by the bow shock. Furthermore, future AAE developments should allow for standoff distance diagnosis, as demonstrated for thermal spray applications (Ref 19), enabling real-time correction of AAE velocity estimations.

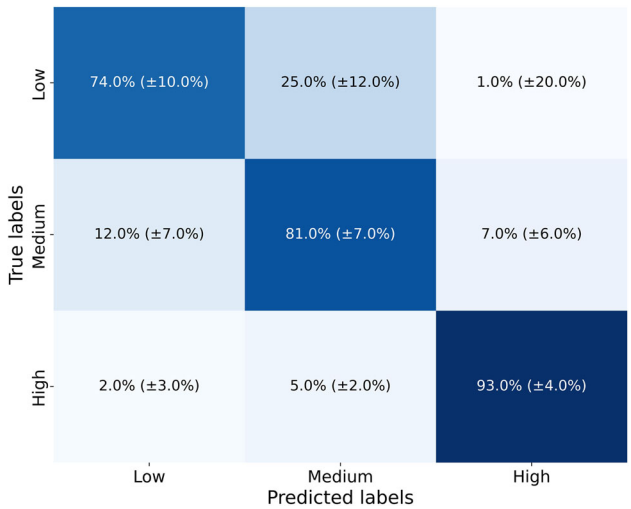

Fig. 17 Average confusion matrix with one standard deviation for the velocity classification model tested with five random initialisations

Conclusions

The feasibility of the AAE for monitoring the cold spray process was investigated. Both statistical and machine learning tools were used to identify the segments where the nozzle is engaged with the substrate and diagnose the spray velocity. The main conclusions are listed below:

- Monitoring the cold spray process using AAE is feasible; it can provide information about the spray velocity and detect when the nozzle is engaged with the substrate.
- The RMS of the signal from the AAE exhibits a positive correlation with the spray velocity, and it can be used to identify permanent shifts in the process conditions for a standardised cold spray process without the need to distinguish spray from overspray segments.
- PSD showed evidence of being agnostic of the pressure and temperature combination that resulted in a specific velocity, reducing the number of experiments required to obtain data for the development of AAE-based process monitoring.
- Although PSD was informative of the spray–overspray condition and the spray velocity, straightforward rule-based models are challenging to develop due to the high variability of the PSD when a short time window is used. To overcome this, larger time windows or more complicated algorithms are required.
- An autoencoder which is trained with the PSD of the spray segments and is agnostic of the overspray segments can identify the spray segments successfully based on its reconstruction error.
- An MLP performed well on diagnostics of the spray velocity. However, further validation is needed with more experimental data.
- While AAE offers a promising, non-intrusive method for real-time monitoring, its accuracy may be affected if the bow shock is not considered in the cases where it is relevant. Incorporating CFD simulations or experimental data to model and quantify the bow shock effect

can enhance the precision of AAE-based velocity estimation.

In summary, the present study suggests the feasibility of using AAE to monitor the key process parameter of impact velocity during a cold spray process. Future studies will focus on refining the diagnostic algorithms and investigating their robustness.

Acknowledgments This work was made possible by funding from the Netherlands Enterprise Agency (RVO), in the framework of the 'Mobiliteitsfonds—Brightsky' project. The experimental part was conducted at the facilities of Titomic Europe B.V.

References

1. M. Yandouzi, S. Gaydos, D. Guo, R. Ghelichi, and B. Jodoin, Aircraft Skin Restoration and Evaluation, *J. Therm. Spray Technol.*, 2014, **23**(8), p 1281-1290.
2. C.A. Widener, M.J. Carter, O.C. Ozdemir, R.H. Hrabe, B. Hoiland, T.E. Stamey, V.K. Champagne, and T.J. Eden, Application of High-Pressure Cold Spray for an Internal Bore Repair of a Navy Valve Actuator, *J. Therm. Spray Technol.*, 2016, **25**(1-2), p 193-201. https://doi.org/10.1007/s11666-015-0366-4
3. A. Astarita, F. Coticelli, and U. Prisco, Repairing of an Engine Block through the Cold Gas Dynamic Spray Technology, *Mater. Res.*, 2016, **19**(6), p 1226-1231.
4. A. Powders, Z. Zhang, X. Sun, S. Huang, X. Han, P. Zhu, and C. Shi, Microstructure, Mechanical Properties and Corrosion Behavior of the Aluminum Alloy Components Repaired by Cold Spray with Al-Based Powders (2021)
5. X. Han, X. Sun, G. Li, S. Huang, P. Zhu, C. Shi, and T. Zhang, A Repair Method for Damage in Aluminum Alloy Structures with the Cold Spray Process, *Materials (Basel)*, 2021, **14**(22), p 1-12.
6. S. Yin, M. Meyer, W. Li, H. Liao, and R. Lupoi, Gas Flow, Particle Acceleration, and Heat Transfer in Cold Spray: A Review, *J. Therm. Spray Technol.*, 2016, **25**(5), p 874-896. https://doi.org/10.1007/s11666-016-0406-8
7. R. Huang and H. Fukanuma, Study of the Influence of Particle Velocity on Adhesive Strength of Cold Spray Deposits, *J. Therm. Spray Technol.*, 2012, **21**(3-4), p 541-549.
8. R.G. Maev, S. Titov, V. Leshchynsky, D. Dzhurinskiy, and M. Lubrick, In Situ Monitoring of Particle Consolidation during Low Pressure Cold Spray by Ultrasonic Techniques, *J. Therm. Spray Technol.*, 2011, **20**(4), p 845-851.
9. S. Yin, X.F. Wang, W.Y. Li, and X.P. Guo, Examination on Substrate Preheating Process in Cold Gas Dynamic Spraying, *J. Therm. Spray Technol.*, 2011, **20**(4), p 852-859.
10. J.G. Legoux, E. Irissou, and C. Moreau, Effect of Substrate Temperature on the Formation Mechanism of Cold-Sprayed Aluminum, Zinc and Tin Coatings, *J. Therm. Spray Technol.*, 2007, **16**(5-6), p 619-626.
11. S.H. Zahiri, T.D. Phan, S.H. Masood, and M. Jahedi, Development of Holistic Three-Dimensional Models for Cold Spray Supersonic Jet, *J. Therm. Spray Technol.*, 2014, **23**(6), p 919-933.
12. H. Koivuluoto, J. Larjo, D. Marini, G. Pulci, and F. Marra, Cold-Sprayed Al6061 Coatings: Online Spray Monitoring and Influence of Process Parameters on Coating Properties, *Coatings*, 2020, **10**(4), p 348. https://doi.org/10.3390/coatings10040348
13. H. Fukanuma, N. Ohno, B. Sun, and R. Huang, In-Flight Particle Velocity Measurements with DPV-2000 in Cold Spray, *Surf. Coatings Technol.*, 2006, **201**(5), p 1935-1941.
14. W. Wang, W. Xue, W. Shufan, M. Zhongcheng, J. Yi, and A.J. Tang, High-Speed Micro-Particle Motion Monitoring Based on Continuous Single-Frame Multi-Exposure Technology, *Materials*, 2022, **15**(11), p 3871. https://doi.org/10.3390/ma15113871
15. M. Alexey Sova, P. Doubenskaia, and I.S. Petrovskiy, Visualization of Particle Jet in Cold Spray by Infrared Camera: Feasibility Tests, *Int. J. Adv. Manuf. Technol.*, 2018, **95**(5-8), p 3057-3063. https://doi.org/10.1007/s00170-017-1435-2
16. Yu. Gbanaibolou Jombo and Zhang, Acoustic-Based Machine Condition Monitoring—Methods and Challenges, *Eng*, 2023, **4**(1), p 47-79. https://doi.org/10.3390/eng4010004
17. A. Burkert, D. Müller, and W. Paa, Acoustic Measurements in a Hexamethyldisiloxane-Loaded Low-Temperature Direct Barrier Discharge (DBD) Plasma Effluent: Nozzle Cleaning, *J. Therm. Spray Technol.*, 2015, **24**(4), p 683-689.
18. Z. Duan, L. Beall, J. Schein, J. Heberlein, and M. Stachowicz, Diagnostics and Modeling of an Argon/Helium Plasma Spray Process, *J. Therm. Spray Technol.*, 2000, **9**(2), p 225-234.
19. S. Kamnis, K. Malamousi, A. Marrs, B. Allcock, and K. Delibasis, Aeroacoustics and Artificial Neural Network Modeling of Airborne Acoustic Emissions During High Kinetic Energy Thermal Spraying, *J. Therm. Spray Technol.*, 2019, **28**(5), p 946-962. https://doi.org/10.1007/s11666-019-00874-0
20. K. Malamousi, K. Delibasis, B. Allcock, and S. Kamnis, Digital Transformation of Thermal and Cold Spray Processes with Emphasis on Machine Learning, *Surf. Coat. Technol.*, 2022, **433**, p 128138. https://doi.org/10.1016/j.surfcoat.2022.128138
21. Y. Lecun, Y. Bengio, and G. Hinton, Deep Learning, *Nature*, 2015, **521**(7553), p 436-444.
22. M. Moradi, A. Broer, J. Chiachío, R. Benedictus, T.H. Loutas, and D. Zarouchas, Intelligent Health Indicator Construction for Prognostics of Composite Structures Utilizing a Semi-Supervised Deep Neural Network and SHM Data, *Eng. Appl. Artif. Int.*, 2023, **117**, p 105502. https://doi.org/10.1016/j.engappai.2022.105502
23. M. Moradi, P. Komninos, R. Benedictus, and D. Zarouchas, Interpretable Neural Network with Limited Weights for Constructing Simple and Explainable HI using SHM Data, *Proc. Annu. Conf. Progn. Heal. Manag. Soc. PHM*, 2022, **14**(1), p 1-11. https://doi.org/10.36001/phmconf.2022.v14i1.3185
24. C.-G. Huang, H.-Z. Huang, Y.-F. Li, and W. Peng, A Novel Deep Convolutional Neural Network-Bootstrap Integrated Method for RUL Prediction of Rolling Bearing, *J. Manuf. Syst.*, 2021, **61**, p 757-772. https://doi.org/10.1016/j.jmsy.2021.03.012
25. Chemical Characteristics of VALIMET Spherical Aluminum Alloy Powders AM 357 AM 2024 AM 2139 AM 2219, Valimet Inc., Stockton, California, USA, (2024)
26. H. Assadi, F. Gärtner, T. Stoltenhoff, and H. Kreye, Bonding Mechanism in Cold Gas Spraying, *Acta Mater.*, 2003, **51**(15), p 4379-4394.
27. T. Schmidt, F. Gärtner, H. Assadi, and H. Kreye, Development of a Generalized Parameter Window for Cold Spray Deposition, *Acta Mater.*, 2006, **54**(3), p 729-742.
28. J. Pattison, S. Celotto, A. Khan, and W. O'Neill, Standoff Distance and Bow Shock Phenomena in the Cold Spray Process, *Surf. Coatings Technol.*, 2008, **202**(8), p 1443-1454.
29. D.P. Kingma and J.L. Ba, Adam: A Method for Stochastic Optimization, 3rd Int. Conf. Learn. Represent. ICLR 2015 - Conf. Track Proc., 2015, pp. 1-15
30. A.L. Maas, A.Y. Hannun, and A.Y. Ng, Rectifier Nonlinearities Improve Neural Network Acoustic Models, *ICML Work. Deep Learn. Audio, Speech Lang. Process.*, **28** (2013)
31. S. Ioffe and C. Szegedy, Batch Normalization: Accelerating Deep Network Training by Reducing Internal Covariate Shift, *32nd Int Conf. Mach. Learn. ICML*, 2015, **2015**(1), p 448-456.
32. N. Srivastava, G. Hinton, A. Krizhevsky, I. Sutskever, and R. Salakhutdinov, Dropout: A Simple Way to Prevent Neural

Networks from Overfitting, *J. Mach. Learn. Res.*, 2014, **15**, p 1929-1958.
33. T.D. Adugna, A. Ramu, and A. Haldorai, A Review of Pattern Recognition and Machine Learning, *J. Mach. Comput.* (2006)